Primljen / Received: 15.3.2026.
Ispravljen / Corrected: 14.5.2026.
Prihvaćen / Accepted: 22.5.2026.
Dostupno online / Available online: 10.8.2026.

Behaviour and bearing capacity of RC columns strengthened with UHPC jackets: the role of interfacial connectors and a predictive model

Authors:

[1]Assoc.Prof. **Julin Wang**, PhD. CE
wangjl_tj@163.com

[1]Assoc.Prof. **Xianhui Li**, PhD. CE
zhanghs0520@163.com
Corresponding author

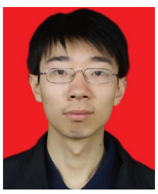

[1]**Wei Liu**, MS. CE
liuwei@sxgkd.edu.cn

[2]**Huanchao Qin**, MS. CE
qinhuanchao@sxgkd.edu.cn

[1]Lecturer **Jing Dong**, MS. CE
dongjing@sxgkd.edu.cn

[1] Shanxi Vocational University of Engineering Science and Technology, China
Faculty of Architectural Engineering
[2] Shanxi Vocational University of Engineering Science and Technology, China
Department for experimental and practical teaching

Research Paper

Julin Wang, Xianhui Li, Wei Liu, Huanchao Qin, Jing Dong

Behaviour and bearing capacity of RC columns strengthened with UHPC jackets: the role of interfacial connectors and a predictive model

Ultra-high-performance concrete (UHPC) is increasingly used as a primary material for strengthening reinforced concrete (RC) columns owing to its ultra-high strength, excellent ductility, durability, and low permeability. However, two key issues remain unaddressed: (1) whether connectors are necessary at the UHPC-to-concrete interface to ensure monolithic behaviour, and (2) the development of a simplified yet accurate model for predicting the bearing capacity of strengthened columns. To address these questions, eight RC columns were tested in two stages. In the first stage, five columns were tested to analyse their failure modes. In the second stage, three specimens validated the numerical model for bearing capacity prediction. Results indicate sufficient steel connectors are required at the UHPC–concrete interface to prevent relative displacement between the UHPC layer and the original concrete, which could otherwise lead to premature structural failure. Moreover, the proposed model demonstrated high accuracy in estimating the bearing capacity of UHPC-strengthened RC columns.

Key words:

UHPC, strengthened RC columns, predictive model, bearing capacity, interfacial connections

Prethodno priopćenje

Julin Wang, Xianhui Li, Wei Liu, Huanchao Qin, Jing Dong

Ponašanje i nosivost AB stupova ojačanih UHPC ovojnicom: uloga spojnih elemenata na sučelju i prediktivni model

Beton ultra velikih svojstava (UHPC) sve se češće primjenjuje kao osnovni materijal za ojačanje armiranobetonskih (AB) stupova zbog svoje iznimno velike čvrstoće, izvrsne duktilnosti, trajnosti i vrlo male propusnosti. Međutim, još uvijek nisu dovoljno razjašnjena dva ključna pitanja: (1) jesu li spojni elementi na sučelju između UHPC-a i postojećeg betona neophodni za osiguranje monolitnog djelovanja te (2) kako razviti pojednostavljeni, ali dovoljno točan model za predviđanje nosivosti ojačanih stupova. Radi odgovora na navedena pitanja provedeno je ispitivanje osam AB stupova u dvije faze. U prvoj fazi ispitano je pet stupova radi analize njihovih mehanizama sloma. U drugoj su fazi tri uzorka korištena za validaciju numeričkog modela za predviđanje nosivosti. Rezultati pokazuju da je na sučelju UHPC-a i betona potrebno osigurati dovoljan broj čeličnih spojnih elemenata kako bi se spriječio relativni pomak između UHPC sloja i izvornog betona, koji bi u suprotnome mogao dovesti do prijevremenoga konstrukcijskog sloma. Nadalje, predloženi model pokazao je visoku razinu točnosti u procjeni nosivosti AB stupova ojačanih UHPC-om.

Ključne riječi:

UHPC, ojačani AB stupovi, prediktivni model, nosivost, spojnice na sučelju

1. Introduction

1.1. Shear strength of concrete-to-concrete interfaces

Achieving quasi-monolithic behaviour in composite members requires that the interface between concretes of different ages possesses sufficient capacity to transfer shear forces. The shear strength at such interfaces is governed by a combination of adhesive bond, friction, aggregate interlock, and dowel action [1, 2, 36–38]. Since the 1960s, extensive research has been conducted worldwide to characterise the shear behaviour of concrete interfaces and inform reliable design and construction practices.

Randl [3] classified the relative displacement between old and new concrete layers as either brittle or ductile. Omar [4] tested eight RC columns strengthened with self-compacting concrete in the absence of interfacial reinforcement; the failure was attributed to the relative slip between the strengthening layer and the original column. Similarly, Gomes et al. [5] tested six columns strengthened with carbon-fibre composites in the tension zone and self-compacting concrete in the compression zone. Their findings emphasised the necessity of connectors at the interface to prevent premature failure owing to relative displacement. Subsequent studies by Sahb [6] and Nascimento [7] confirmed that an adequate number of steel connectors between the reinforcement layer and the original column effectively prevented damage caused by interfacial slip.

In the absence of tensile stress normal to the interface, an anchorage length of 6d (where d is the connector diameter) in the concrete, whether cast in-situ or equivalent, is sufficient to mobilise the shear resistance of the connector fully [8].

1.2. UHPC-strengthened columns

RC columns are susceptible to steel corrosion induced by carbonation or inadequate concrete compaction, which can significantly reduce their load-bearing capacity, necessitating urgent strengthening. Traditional retrofitting techniques, such as steel plate bonding, conventional concrete jacketing, and fibre-reinforced polymer (FRP) wrapping, have been widely used; however, they exhibit notable drawbacks. Steel plates are prone to corrosion [9], FRP materials suffer from poor high-temperature performance and high cost [10], and concrete jacketing adds considerable weight to existing structures [11, 12].

In contrast, ultra-high-performance concrete (UHPC) offers a superior combination of properties, including ultra-high compressive and tensile strengths, excellent ductility, fire resistance, outstanding workability, low permeability, and a high strength-to-weight ratio [13–17]. These characteristics make UHPC particularly suitable for strengthening RC components.

Numerous experimental studies [18–22] have demonstrated that externally applied UHPC jackets can substantially enhance the load-bearing capacity and ductility of RC columns. Dadvar et al. [23] proposed a predictive model for the stress–strain behaviour of UHPC-jacketed RC columns. Lampropoulos et al. [24] conducted numerical analyses to evaluate the influence of key parameters, such as jacket thickness and concrete shrinkage, and compared the performance of UHPC jackets with that of conventional concrete jackets.

1.3. Objectives of the paper

Necessity and minimum number of steel connectors

The effective transfer of shear forces across the UHPC–concrete interface is essential for achieving quasi-monolithic behaviour in RC columns strengthened with UHPC jackets, thus constituting a critical design consideration. However, installing connectors on existing concrete surfaces is time-consuming and technically demanding. Therefore, this study addresses the following questions through an experimental investigation: are interfacial connectors necessary, or can they be omitted? If required, what is the minimum number of connectors to ensure adequate performance?

Predictive model for the bearing capacity of RC columns strengthened with UHPC jackets

Although UHPC has been extensively studied and successfully applied as a repair material for structural components, limited research has focused on the numerical modelling of RC columns strengthened with UHPC jackets. To address this gap, this paper proposes a simplified model to predict the bearing capacity of strengthened columns. The accuracy and reliability of the model were validated by comparing it with experimental results..

2. Experimental program

2.1. Specimen details and test plan

Eight column specimens were tested in this experiment; their geometric details are shown in Figure 1. The specimens were fabricated in two stages: five were constructed in the first stage and three in the second stage.

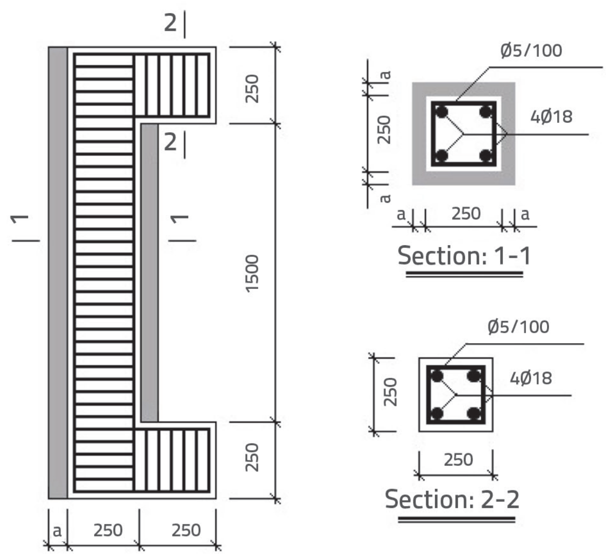

Figure 1. Geometry and reinforcement layout of specimens (The grey regions indicate the UHPC jacket, and the white region indicates the original RC column; The parameter 'a' denotes the thickness of the UHPC jacket; unit: mm)

Table 1. Specifications of specimen columns

Columns		Dimensions before reinforcement [mm]	Thickness of UHPC jackets: a [mm]	Spacing between connectors [mm]
First stage	C1	250 × 250	-	-
	C2	250 × 250	15	-
	C3	250 × 250	15	400
	C4	250 × 250	15	300
	C5	250 × 250	15	200
Second stage	C6	250 × 250	25	200
	C7	250 × 250	40	200
		250 × 250	50	200

In the first stage, one unstrengthened specimen served as a reference, whereas the other four were strengthened with 15 mm thick UHPC jackets. As the load application point remained unchanged while the UHPC jacket increased the cross-sectional dimensions, the actual eccentricity relative to the centroid of the strengthened section became smaller than the original eccentricity of 125 mm. To investigate the effect of steel connectors on achieving quasi-monolithic behaviour between the UHPC jacket and the original column, three of the four strengthened specimens (C3, C4, and C5) were provided with varying quantities of connectors (spacings of 400, 300, and 200 mm, respectively), while one specimen (C2) had no connectors.

In the second stage, three additional specimens were tested to evaluate the bearing capacity of the strengthened columns with different jacket thicknesses. These specimens featured UHPC jackets with thicknesses of 25, 40, and 50 mm, each with a uniform connector spacing of 200 mm. Before applying the UHPC layer, the surface of the RC column was roughened by sandblasting. The steel connectors, which were fabricated from the same material as the column stirrups, had a diameter of 5.0 mm. The configuration and dimensions of the connectors are shown in Figure 2.

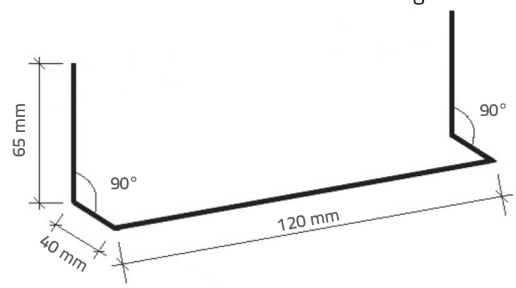

Figure 2. Connector configuration and dimensions

To fix the connectors to the existing reinforcement, grooves were cut on the tensile and compressive faces to expose the stirrups. This ensured that the connectors remained in position during the UHPC pouring, as shown in Figure 3. The details of the test specimens are presented in Table 1.

Figure 3. Placement of a connector

2.2. Material properties

To determine the actual axial compressive strength of the RC columns, three standard cubic specimens (150 ×150 ×150 mm) were cast from the same batch and tested after 28 days of curing under the same conditions as the columns. The average compressive strength of the three cubes was 32.0 MPa. The material properties of the steel reinforcements are listed in Table 2. The mixture proportions and mechanical properties of UHPC are listed in Tables 3 and 4, respectively. Hooked-end steel fibres with a tensile strength of 1350 MPa (yield strength of 1100 MPa), measuring 13 mm in length and 0.20 mm in diameter, were used in the experiments.

Table 2. Mechanical properties of steel bars

Steel grades	Diameter [mm]	Yield strength [MPa]	Tensile strength [MPa]	Elastic modulus [MPa]
HRB400	5	470.3	650.1	2.0×10^5
HRB500	18	544.2	730.2	2.0×10^5
Note: HRB400 and HRB500 denote hot-rolled ribbed bars with yield strength characteristic values of 400 MPa and 500 MPa. respectively				

Table 3. Mixture composition of UHPC per cubic metre [m³]

Ingredients	Cement	Water	Silica	Quartz sand	Superplasticizer	Steel fibres
Quantity [kg]	900	165	216	1004	42	160

Table 4. Mechanical properties of UHPC

Compressive strength [MPa]	Tensile strength [MPa]	Ultimate tensile strain	Ultimate compressive strain
149.5	17.4	0.0125	0.0038

2.3. Arrangement of measurement points

2.3.1. Horizontal deflection

To measure the horizontal displacement of the specimens, five displacement transducers were vertically aligned on the tension side from top to bottom, as shown in Figure 4. The deflection meters have an accuracy of 0.01 mm and a reading range of 0 to 60 mm.

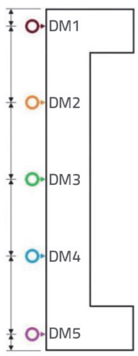

Figure 4. Schematic diagram of the deflection metre distribution

2.3.2. Strain of the longitudinal reinforcements

To monitor the deformation of the longitudinal reinforcements in the specimens, strain gauges were installed at the mid-height of the columns. Strain gauges were affixed to the interior surfaces of the longitudinal reinforcements, as shown in Figure 5.

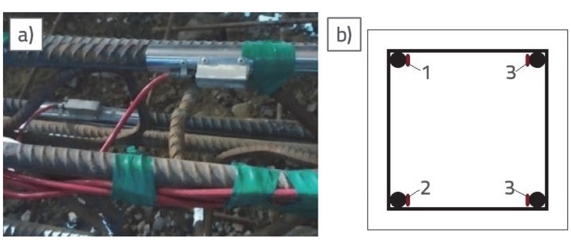

Figure 5. a) Photo of strain gauges; b) Positions of strain gauges

2.3.3. Concrete and UHPC strain measurement

To measure the strain distribution across the specimen cross-sections during testing, five strain gauges were installed along the midheight on the side parallel to the plane of bending for the strengthened specimens (C2–C8), whereas three strain gauges were used for the unstrengthened specimen C1 (Figure 6). The strain data were collected using an LD8174-1G14 static strain acquisition instrument.

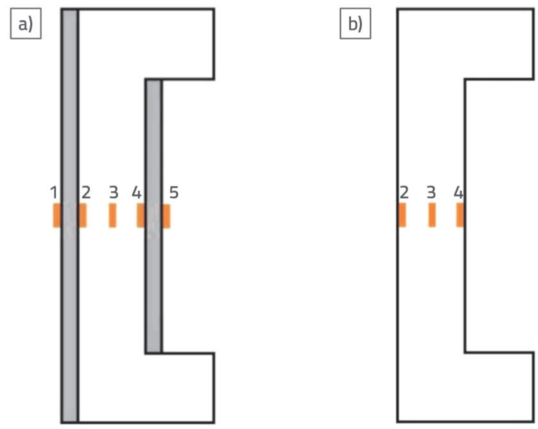

Figure 6. Strain gauge positions: a) strengthened columns; b) non-strengthened column

2.3.4. Relative displacement between UHPC jackets and RC columns

Five linear variable differential transformers (LVDTs) were used on each strengthened column to measure the relative displacement between the UHPC jackets and the RC columns (Each LVDT was fixed to the UHPC jacket surface using a magnetic base or small bracket).

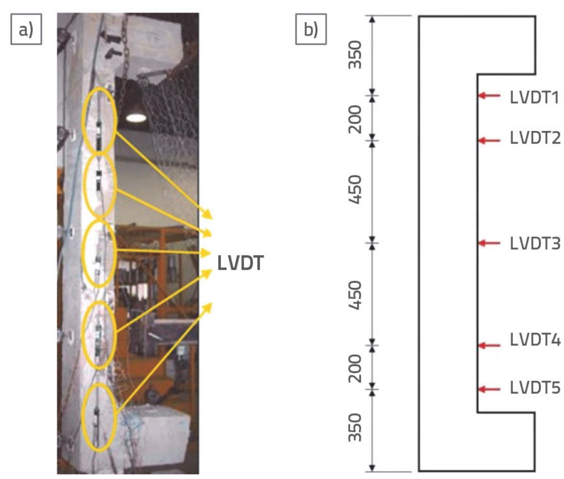

Figure 7. LVDTs: a) Photo; b) Locations

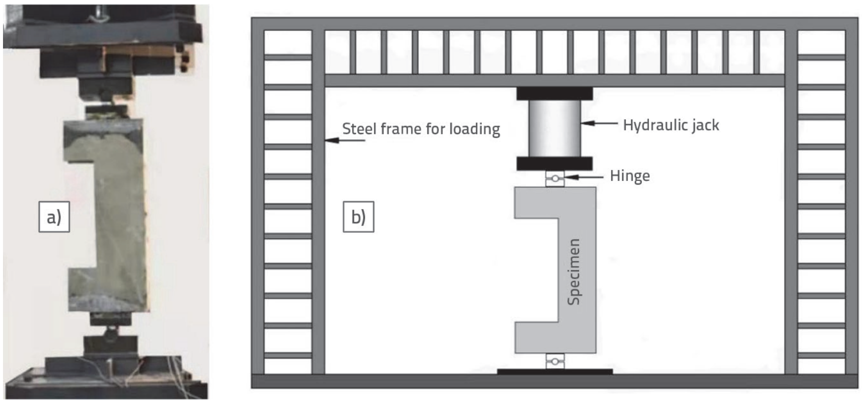

Figure 8. Loading apparatus: a) Test photo; b) Schematic diagram

The tip of the LVDT probe was placed in light contact with a small steel plate that was glued to the surface of the original RC column. Thus, the LVDT measured the displacement of the original column relative to the UHPC jacket. The locations of the LVDTs are shown in Figure 7.

2.4. Test loading device

The tests were conducted at the Structural Laboratory of Shanxi Vocational University of Engineering Science and Technology. A 500-ton servohydraulic jack vertically fixed between the top and bottom ends of the specimens was used to apply the load. The upper end of the specimen featured a hinge connection to the jack, whereas the lower end was connected via a hinge to a 15 mm thick steel base plate, as illustrated in Figure 8.
Following the test specifications [25], loading proceeded under load control. All the columns were initially loaded in 10 kN increments until the first crack appeared. The loading rate was maintained at approximately 2 kN/min during the loadcontrol stage. Subsequently, the load increment was increased to 20 kN. To ensure specimen stability and prevent misalignment or falling prior to the main test, a 5 kN preload was applied.

3. Experimental findings and analysis

3.1. Experimental phenomena

Specimen C1
Specimen C1 served as the non-strengthened reference column with an eccentricity of e = 125 mm and cross-sectional dimensions of 250 ×250 mm. During the initial loading phase, the specimen remained elastic. Upon reaching a load of 135 kN, the first transverse crack was initiated on the tensile face at mid-height, measuring approximately 100 mm in length and 0.02 mm in width. As the load increased to 275 kN, six transverse cracks developed uniformly along the tensile face of the column and propagated toward the compressive side. At an ultimate load of 560 kN, the longitudinal tensile reinforcement in the tensile zone yielded. Simultaneously, concrete crushing occurred in the compressive zone, accompanied by outward buckling and spalling of the concrete surface, which led to specimen failure.

Specimen C2
Specimen C2, a strengthened column with a 280 mm×280 mm cross section and a 15 mm-thick UHPC jacket, was tested under an eccentricity (e) of 125 mm. No connectors were present at the concrete–UHPC interface. During the initial loading, C2 exhibited elastic behaviour similar to that of specimen C1. Upon reaching 410 kN, cracks were formed on the tension face of the original column. Simultaneously, fine and densely spaced vertical cracks appeared on the tensile side of the UHPC layer. When the load increased to 710 kN, a sudden local peel-off occurred between the compressed UHPC layer and the original concrete, accompanied by a slight audible "pop" sound. Subsequently, at 730 kN, the tension zone reinforcing bars yielded, prompting the termination of the test.

Specimen C3
For Specimen C3, steel shear connectors were installed at a spacing of 400 mm along each row at the concrete–UHPC interface. All other conditions were identical to those used for Specimen C2. Initially, the specimen exhibited an elastic behaviour under loading. When the load reached 500 kN, vertical cracks developed on the tension side of the UHPC layer at the mid-height. With a further increase in the load, these initial cracks propagated rapidly along the longitudinal axis of the column. Upon reaching 830 kN, localised separation occurred between the UHPC layer on the compression side and the existing concrete column.

Specimen C4
The steel shear connectors were spaced 300 mm along each row at the concrete–UHPC interface, with the other conditions identical to those of Specimen C3. The specimen exhibited a behaviour similar to that of specimen C3 until the loading reached 890 kN, when a relative displacement occurred between the UHPC layer and concrete in the compression zone.

Specimen C5
For Specimen C5, the steel connectors were spaced at 200 mm per row. All the other conditions were identical to those of Specimen C4. Initially, the specimen exhibited an elastic behaviour under loading. At a load of 690 kN, several microcracks emerged on the tensile side of the UHPC layer. Upon reaching 960 kN, localised spalling occurred in the compression zone of the original column, accompanied by a brittle failure sound. As the loading increased to 1020 kN, local fibres within the compression zone of the UHPC layer were pulled out and fractured, generating a slight cracking sound and resulting in numerous dense longitudinal splitting cracks. Loading was subsequently discontinued.

Specimens C6, C7 and C8

Specimens C6, C7, and C8 represent the second stage of the experiment. Following the completion of the first-stage tests, these specimens were produced, cured, and tested. The UHPC layer thicknesses for C6, C7, and C8 were 25, 40, and 50 mm, respectively. All other conditions were identical to those of specimen C5. Failure occurred in specimens C6, C7, and C8 at applied loads of 1100, 1350, and 1590 kN, respectively. Failure was characterised by the crushing of both the concrete and UHPC within the compression zone. No relative displacement was observed between the UHPC and the original column during testing.

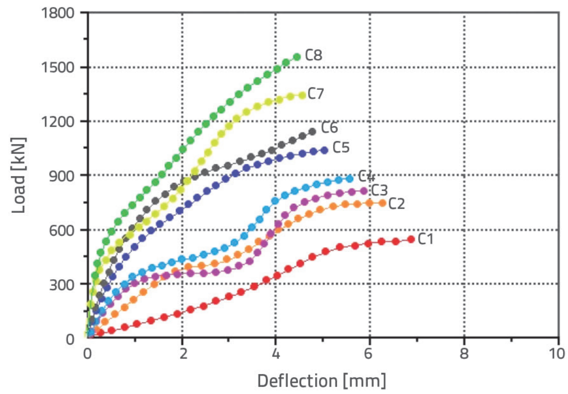

Figure 9. Comparison of load-deflection curves of the specimens

3.2. Horizontal displacement of the specimens

The lateral deflection curves at mid-height for all the specimens are presented in Figure 9. This figure shows that, during the initial loading stage, the deflection rate decreased for specimens C1–C8. At the peak load, specimen C8 exhibited the smallest deflection (4.4 mm), whereas specimen C1 exhibited the largest. The deflections of specimens C2–C7 decreased progressively between these values. This behaviour is primarily attributed to two factors: (1) UHPC possesses a significantly higher elastic modulus and compressive strength than ordinary concrete. Increasing the UHPC layer thickness increased the cross-sectional area, thereby enhancing column stiffness, reducing deflection, and increasing load-bearing capacity. (2) Sufficient connectors are crucial for ensuring an effective force transfer at the UHPC–concrete interface, enabling composite action between the UHPC layer and underlying reinforced concrete (RC) column. This composite action further increases the bearing capacity, stiffness, and ductility of the reinforced columns.

3.3. Deformation of longitudinal reinforcements

For each specimen, the strain gauges were attached to the inner sides of the steel bars. The deformation in the tensile steel bars was measured using gauges 1 and 2, whereas the compressive deformation was monitored using gauges 3 and 4. The red dotted line indicates the yield deformation of the longitudinal steel bars (2.45 mm/m). Figure 10 illustrates the load-deformation response of the longitudinal reinforcements across all specimens.

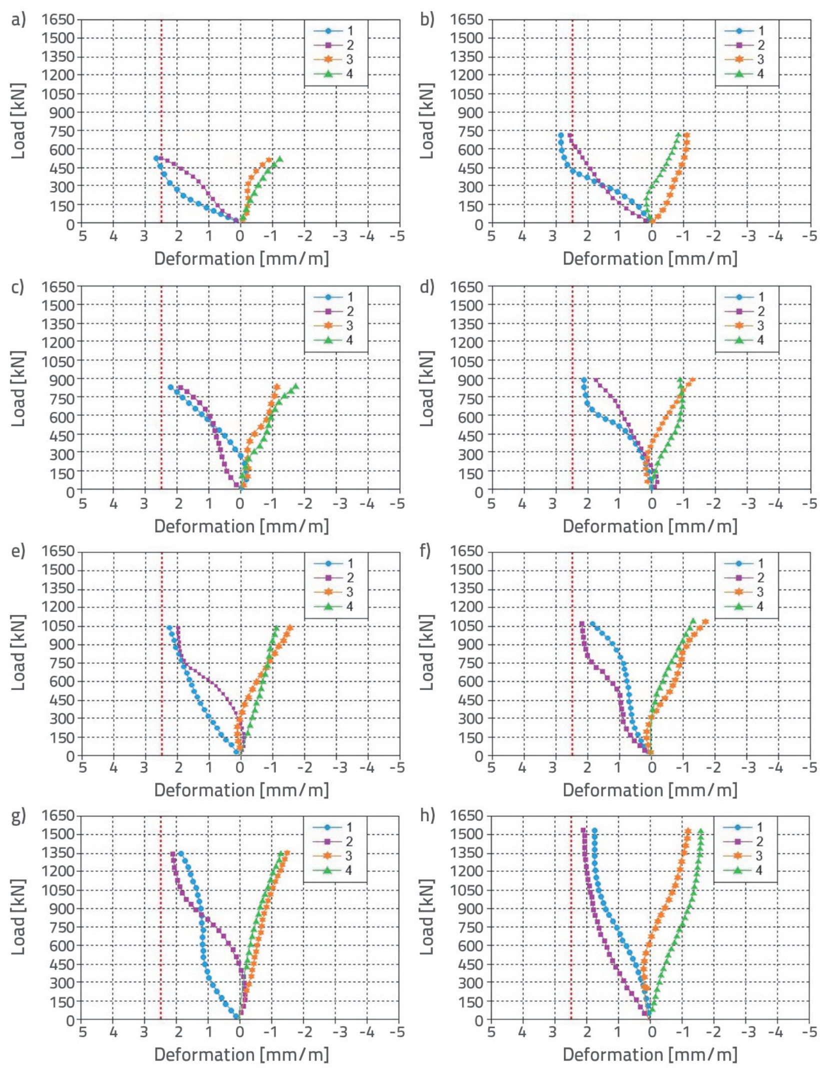

Figure 10. Load-deformation curves for longitudinal reinforcements of: a) C1; b) C2; c) C3; d) C4; e) C5; f) C6; g) C7; h) C8

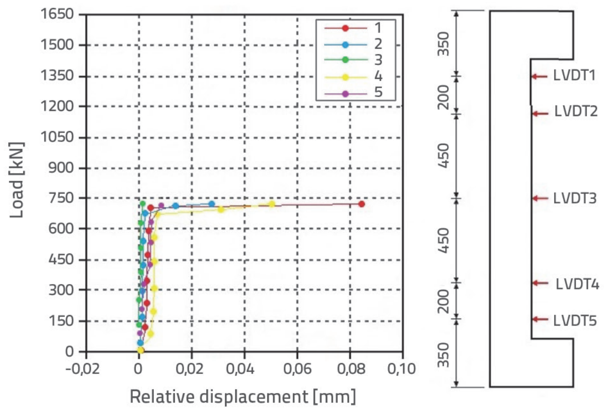

Figure 11. Relative displacements of Specimen C2

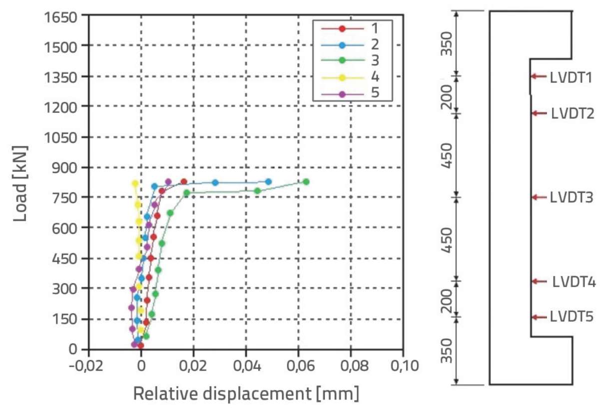

Figure 12. Relative displacements of Specimen C3

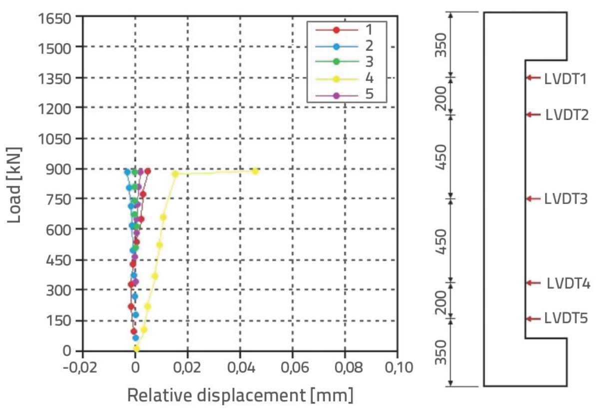

Figure 13. Relative displacements of Specimen C4

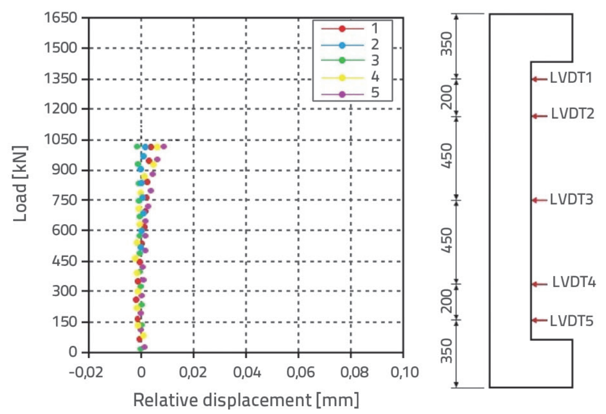

Figure 14. Relative displacements of Specimen C5

3.4. LVDT measurement results

Figures 11 to 14 present the relative displacements between the UHPC jackets and concrete for specimens C2, C3, C4, and C5. Key observations include the following:

- Specimen C2 exhibited maximum relative displacement (0.086 mm) at measurement point 1.
- Specimen C3 showed peak relative displacement (0.064 mm) at measurement point 3.
- Specimen C4 reached its maximum (0.047 mm) at measurement point 4.
- Specimen C5 demonstrated negligible displacement (0.007 mm), effectively indicating no interfacial movement.

These results establish that specimen C2 (with no connectors) and specimens C3/C4 (with insufficient connectors) experienced significant UHPC–concrete slip. This interfacial displacement critically compromises UHPC material performance.

3.5. UHPC and concrete strain

To verify compliance with the plane section assumption in the UHPC-strengthened eccentrically compressed columns, three to six strain gauges were installed along the mid-height on the side parallel to the bending plane. Figures 15 and 16 show the strain distributions along the mid-height of specimens C5 and C6, respectively. These figures indicate that the plane-section assumption holds true under lower loads. As the loading increased, the strain distribution gradually deviated from linearity but remained approximately linear. This demonstrates that eccentrically compressed columns reinforced with UHPC and equipped with sufficient connectors between the UHPC and concrete interfaces satisfy the plane section assumption. This finding provides a theoretical basis for subsequent numerical analyses of such members.

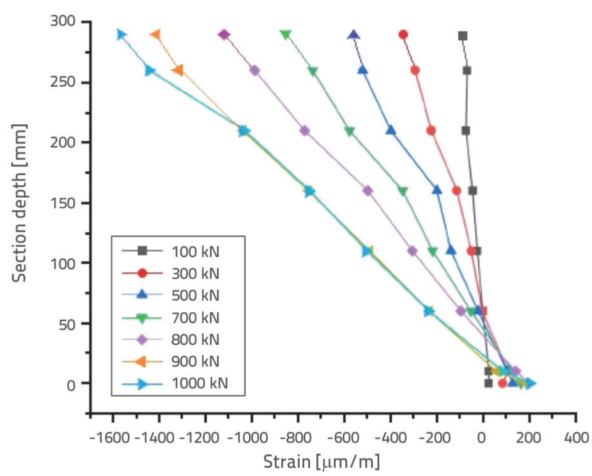

Figure 15. Concrete/UHPC strain in the middle section of C5

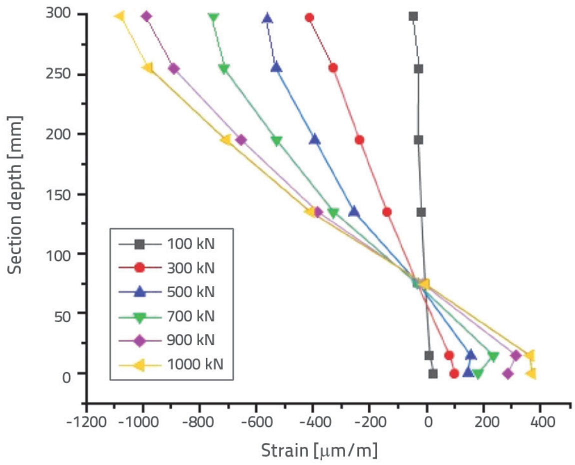

Figure 16. Concrete/UHPC strain in the middle section of C6

3.6. Detailed analysis of failure mechanisms

3.6.1. Local separation of the UHPC jacket

The LVDT measurements (Figures 11 to 14) provided quantitative evidence of interfacial debonding. For specimen C2 (no connectors), the maximum relative displacement reached 0.086 mm at measurement point 1, indicating a significant slip between the UHPC jacket and the original concrete. This slip was initiated at midheight on the tension side and rapidly propagated along the interface, leading to the premature local separation of the jacket on the compression side at 710 kN (see Section 3.1). For specimens C3 (connector spacing of 400 mm) and C4 (300 mm), the maximum relative displacements were 0.064 and 0.047 mm, respectively. Although these values are lower than those of specimen C2, they still reflect an insufficient interfacial shear transfer. In both specimens, local separation still occurred on the compression side (at 830 kN for C3 and 890 kN for C4), but the onset of debonding was delayed compared with specimen C2. In contrast, specimen C5 (connector spacing of 200 mm) exhibited a maximum relative displacement of only 0.007 mm, which was negligible and indicated quasi-monolithic behaviour. No visible interfacial separation was observed during loading. These results demonstrate that a connector spacing of 200 mm is sufficient to suppress the local debonding and ensure full composite action.

3.6.2. Influence of eccentricity

All specimens were tested under the same nominal eccentricity e_{nom} = 125 mm, defined as the distance from the load application point to the centroid of the original RC column crosssection (250 mm×250 mm). However, after applying the UHPC jacket, the cross-sectional dimensions increased (e.g., to 280 mm×280 mm for C2–C5 and even larger for C6–C8), whereas the load application point remained unchanged. Consequently, the eccentricity relative to the centroid of the strengthened section decreased.

For a symmetrically applied jacket (equal thickness on both sides), the centroid shift was zero. However, the increased section modulus and moment of inertia reduced the bending moment per unit strain. More importantly, a smaller actual eccentricity led to a higher axial load capacity for the same material strength. This effect partially explains the progressive increase in the failure loads from specimens C5 (1020 kN) to C8 (1590 kN), even when the jacket thickness exceeds that required for optimal connector performance.

3.6.3. Mechanical interpretation of composite action

The strain gauge data from the midheight sections (Figures 15 and 16 for C5 and C6, respectively) confirm that the plane section assumption approximately holds under service loads, justifying the use of a sectional analysis. The degree of the composite action depends critically on the number of interfacial connectors. When the connectors were absent (C2) or insufficient (C3, C4), the UHPC jacket and the original column could not develop full strain compatibility. As a result, the jacket acted as an independent external layer that carried compression only after a substantial slip had occurred. The shear force at the interface is primarily transferred through friction and weak adhesive bonds, which are unreliable. Once the local bond was exhausted, sudden debonding occurred on the compression side (where the compressive stress created a shear flow along the interface). This debonding propagates rapidly because the absence of sufficient connectors does not provide a crackarrest mechanism.

In contrast, with a connector spacing of 200 mm (C5–C8), the steel connectors acted as dowels that directly transferred shear across the interface. The connectors also provide a clamping action, increasing the frictional resistance. The measured degree of joint reinforcement was sufficient to ensure that the shear strength of the interface exceeded the maximum shear flow induced by the applied load. Under these conditions, the UHPC jacket and original column behaved monolithically, and the strengthened column could be designed using the conventional RC theory with a composite section.

Furthermore, the tensile strength of the UHPC (17.4 MPa, Table 4) contributes to resisting bending moments, particularly on the tension side. In C5–C8, because no interfacial slip occurred, the UHPC layer on the tension side remained intact and participated in the tension-stiffening, delaying the yielding of the longitudinal steel bars. This is evident from the load-deformation curves of the tensile reinforcements (Fig. 10, C5–C8), which exhibited a higher yield load than the specimens with insufficient connectors.

4. Address the first research question posed in Section 1

The experimental results indicated that retrofitting eccentrically compressed RC columns with externally attached UHPC solely relying on interface bonding without installing connectors is unreliable and inefficient. Under these conditions, interface peeling invariably emerges as the primary failure mode. This significantly compromises the performance of UHPC and can lead to catastrophic brittle failure. Furthermore, an insufficient number of connectors severely compromises the reinforcing effectiveness of UHPC. This causes the retrofitted columns to undergo premature brittle failure, predominantly tilizerized by interface separation, thereby failing to fully tilize the high strength and superior mechanical properties of UHPC.
In the experiment, we also found that within the range of the parameters tested, a connector spacing of 200 mm was necessary to achieve quasi-monolithic behaviour. This result is consistent with those obtained by Nascimento et al. [7, 26, 27, 28] in their experimental studies.

5. Predictive model

This section presents the calculation model for investigating the load-bearing capacity of RC columns strengthened with UHPC jackets.

5.1. Basic assumptions

To simplify the model formulation and analysis, the following assumptions are made:
- The plane sections remain planar after bending deformation in the UHPC-strengthened column. (This hypothesis is validated in Section 3).
- The tensile strength of conventional concrete is neglected.
- A perfect bond is assumed between the steel reinforcement and both conventional concrete and UHPC.
- The tensile force in the cross-sections is jointly resisted by the steel reinforcement and the UHPC.

5.2. Constitutional relationship of materials

5.2.1 Concrete

This study adopts the stress–strain relationship for concrete proposed in [29] and illustrated in Figure 17, expressed as:

$$\sigma = \begin{cases} E_c\varepsilon \dfrac{f_c/(E_c\varepsilon_0 - f_c)}{f_c/(E_c\varepsilon_0 - f_c) + (\varepsilon/\varepsilon_0)^{E_c\varepsilon_0/(E_c\varepsilon_0 - f_c)}} & 0 \le \varepsilon \le \varepsilon_0 \\ \dfrac{\varepsilon f_c}{\alpha_c(\varepsilon - \varepsilon_0)^2/\varepsilon_0 + \varepsilon} & \varepsilon_0 < \varepsilon \le \varepsilon_{cu} \end{cases} \quad (1)$$

where:
E_c – is the elastic modulus of concrete
f_c – is the compressive strength of concrete
ε_0 – is the strain corresponding to the peak stress f_c
ε_{cu} – is the ultimate strain corresponding to a stress level of 0,5 f_c on the descending branch of the compressive stress-strain curve
α_c – is a parameter governing the descending branch.

The value of which depends on f_c as described in Table 5.

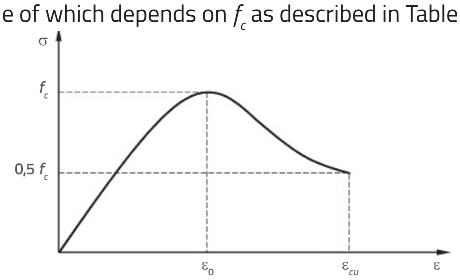

Figure 17. Compressive stress-strain curve of concrete

5.2.2. UHPC

1. Compressive stress–strain relationships
The compressive stress–strain relationship for the UHPC, as illustrated in Figure 18a), is described by the following equation [30]:

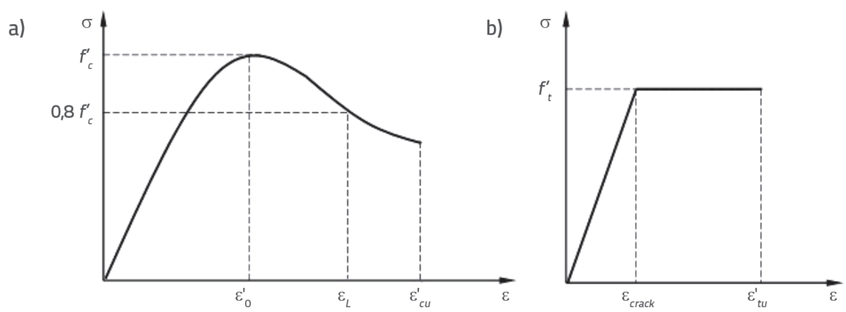

Figure 18. Stress–strain curve of UHPC: a) compression; b) tension

Table 5. Values of α_c

f_c [N/mm²]	20	25	30	35	40	45	50	55	60	65	70	75	80
α_c	0.74	1.06	1.36	1.65	1.94	2.21	2.48	2.74	3.00	3.25	3.50	3.75	3.99

$$\sigma = \begin{cases} E_c \varepsilon \dfrac{f_c/(E_c\varepsilon_0 - f_c)}{f_c/(E_c\varepsilon_0 - f_c) + (\varepsilon/\varepsilon_0)^{E_c\varepsilon_0/(E_c\varepsilon_0 - f_c)}} & 0 \le \varepsilon \le \varepsilon_0 \\ \dfrac{\varepsilon f_c}{\alpha_c(\varepsilon-\varepsilon_0)^2/\varepsilon_0 + \varepsilon} & \varepsilon_0 < \varepsilon \le \varepsilon_{cu} \end{cases} \quad (2)$$

where:

$f_c^{'}$ – compressive strength of UHPC
$E_{initial}$ – initial modulus of elasticity of UHPC
$E_0 = f_c^{'} / \varepsilon_0^{'}$ – secant modulus at the peak stress $f_c^{'}$
$\varepsilon_0^{'}$ – strain at the peak stress $f_c^{'}$
$\varepsilon_{cu}^{'}$ – ultimate compressive strain.

The value of the ultimate compressive deformation is taken as 0.0035 for a fibre volume fraction of 1.0 % and 0.004 for fibre volume fractions between 1 % and 3 % [31]. ε_L is the strain corresponding to a stress value of 0,8 $f_c^{'}$ on the descending branch of the compressive stress-strain curve, which can be calculated by the following equation (3) [32]:

$$\varepsilon_L = \varepsilon_0' \left[0.125 \frac{E_{initial}}{E_0} + 0.8 + \sqrt{\left(0.125 \frac{E_{initial}}{E_0} + 0.8\right)^2 - 0.8} \right] \quad (3)$$

2. Tensile stress–strain relationships

To simplify the proposed model, the tensile behaviour of UHPC [33] was modelled, as shown in Figure 18.b.

$$\sigma = \begin{cases} f_t' \dfrac{\varepsilon}{\varepsilon_{crack}} & 0 \le \varepsilon \le \varepsilon_{crack} \\ f_t' & \varepsilon_{crack} < \varepsilon \le \varepsilon_{tu}' \end{cases} \quad (4)$$

where ε_{crack} represents the tensile strain at crack initiation, $\varepsilon_{tu}^{'}$ is the ultimate tensile strain (taken as 0.01H according to [33], where H is the height of the column section), and f_t' is the tensile strength calculated using the following equation (5) [34]:

$$f_t' = \eta_0 \eta_l \tau_f V_f \frac{l_f}{d_f} \quad (5)$$

where:

η - s the effective direction coefficient of the steel fibre (0,35 – 0,50) [34]
η_l – length efficiency factor of the steel fibre
V_f – fibre volume fraction
l_f – fibre length
d_f – fibre diameter
τ – rigid-plastic bond strength (determined experimentally).

5.2.3. Steel bars

The stress-strain relationship of the steel bars was modelled using an ideal elastoplastic model, expressed as follows:

$$\sigma = \begin{cases} \varepsilon E_s & \varepsilon \le \varepsilon_y \\ f_y & \varepsilon_y < \varepsilon \le \varepsilon_{su} \end{cases} \quad (6)$$

where E_s is the elastic modulus of steel, f_y is the tensile strength of steel, ε_y is the yield strain corresponding to f_y, and ε_{su} is the ultimate strain of steel.

5.3. Equivalent rectangular stress block

For flexure-compression members, the stress distribution of concrete or UHPC in the compression zone can be simplified into an equivalent rectangular stress block, as illustrated in Figure 19 [29, 35]. In this figure, B is total width of the strengthened crosssection; H is total height of the strengthened crosssection; h_0 is effective depth of the longitudinal tension reinforcement (distance from compression face to centroid of tension steel); x denotes the depth of the compression zone; x_c is the distance from the location of the first crack to the neutral axis; a represents the thickness of the UHPC jackets; A_s and A_s' are the cross-sectional areas of the tensile and compressive reinforcing bars, respectively; e is the eccentric distance; N is the applied eccentric compressive load; f_c is the axial compressive strength of concrete; f_y and f_y' are the yield strengths of tensile and compressive steel reinforcements, respectively; f_c' and f_t' are the compressive and tensile strengths of UHPC.

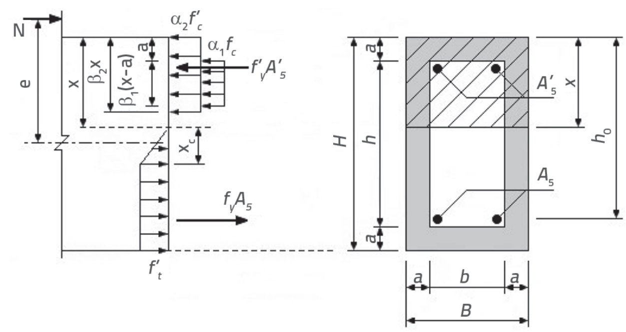

Figure 19. Stress distribution of UHPC-strengthened columns

Coefficients α_1, α_2, β_1 and β_2 define the stress block geometry, calculated as follows [29, 35]:

$$\alpha_1 = \begin{cases} 1.0 & f_c \le 23.1 \text{ MPa} \\ 0.94 + \dfrac{0.06(35.9 - f_c)}{12.8} & 23.1. \text{ MPa} < f_c < 35.9 \text{ MPa} \\ 0.94 & f_c = 35.9 \text{ MPa} \end{cases} \quad (7)$$

$$\alpha_2 = \begin{cases} 0.85 & f_c' \le 69 \text{ MPa} \\ 0.85 - 0.0029(f_c' - 69) \ge 0.75 & f_c' > 69 \text{ MPa} \end{cases} \quad (8)$$

$$\beta_1 = \begin{cases} 0.80 & f_c \le 23.1 \text{ MPa} \\ 0.74 + \dfrac{0.06(35.9 - f_c)}{12.8} & 23.1. \text{ MPa} < f_c < 35.9 \text{ MPa} \\ 0.74 & f_c = 35.9 \text{ MPa} \end{cases} \quad (9)$$

$$\beta_2 = \begin{cases} 0.85 & f_c' \leq 28 \text{ MPa} \\ 0.85 - 0.007252\left(f_c' - 28\right) \geq 0.65 & f_c' > 28 \text{ MPa} \end{cases} \tag{10}$$

5.4. Bearing capacity of a reinforced column

According to Figure 19, the bearing capacity of a reinforced column should comply with the following formulae:

$$N \leq \alpha_1\beta_1 f_c\left(x-a\right)b + \alpha_2 f_c' a\left(B + 2\left(\beta_2 x - a\right)\right) + f_y' A_s' - f_y A_s - f_t'\left(x_c + 2\left(H - x - x_c - a\right) + B\right) \tag{11}$$

$$\begin{aligned} Ne \leq{} & \alpha_1\beta_1 f_c\left(x-a\right)b\left(x - a - \frac{\beta_1 x}{2}\right) + \alpha_2 f_c' aB\left(x - \frac{a}{2}\right) + \\ & 2\alpha_2 f_c' a\left(\beta_2 x - a\right)\left(x - \frac{\beta_2\left(x+a\right)}{2}\right) + f_y' A_s'\left(h_0 + x - H\right) + \\ & f_y A_s\left(h_0 - x\right) + \frac{2}{3} f_t' a x_c^2 + f_t' a\left(H - x - x_c - a\right)\left(H - x + x_c - a\right) + \\ & f_t' aB\left(H - x - \frac{x}{2}\right) \end{aligned} \tag{12}$$

Equations (11) and (12) are solved simultaneously for a given crosssection and material properties. Because the neutral axis depth x was unknown, an iterative approach was used:
- Assume an initial value of x (usually between 0 and H);
- Compute the strains in all materials using the plane section assumption;
- Obtain stresses from the constitutive laws (Section 5.2);
- Calculate the internal force resultants (concrete, UHPC, and steel in tension and compression)
- Check the equilibrium: sum of horizontal forces = 0 (equation (11)) and moment equilibrium about the centroid (equation (12)).
- Adjust x and repeat until equilibrium is satisfied within a tolerance;
- The corresponding *N* is the predicted ultimate bearing capacity.

5.5. Comparison of predicted and experimental values

To validate the accuracy of the proposed bearing capacity formulas for reinforced concrete columns, the predicted values were compared with the experimental results, as summarised in Table 6. The table demonstrates good agreement between the calculated and experimental values.

6. Conclusion

This study investigated the monolithic behaviour and ultimate bearing capacity of reinforced concrete (RC) columns strengthened with UHPC jackets. By testing eight column specimens and subsequent analytical modelling, the following key conclusions can be drawn:

Critical Role of Shear Connectors: Experimental results unequivocally demonstrate that achieving effective composite action and monolithic behaviour between the existing RC column and the external UHPC jacket is critically dependent on the provision of adequate shear connectors at the interface. Specimens without connectors exhibited premature failure, characterised by significant interfacial debonding and delamination of the UHPC jacket, severely limiting the exploitation of UHPC's superior strength and its overall strengthening effectiveness. This finding highlights that shear connectors are not optional but are essential for ensuring force transfer and developing the full potential of UHPC-strengthened RC columns.

Validated Analytical Model for Bearing Capacity: A rational analytical model is proposed to predict the ultimate axial bearing capacity of RC columns strengthened with external UHPC jackets that incorporate shear connectors. The model explicitly accounts for the contributions of both the original RC core and UHPC jacket, considering the enhanced confinement and composite action facilitated by the connectors. The accuracy of the proposed model was rigorously validated against experimental data. The predicted failure loads were in excellent agreement with the measured values. This strong correlation confirms the reliability of the model for practical design applications.

Effective Strengthening Technique: When equipped with properly designed shear connectors, external UHPC jackets proved to be highly effective in significantly enhancing the

Table 6. Comparison of predicted and experimental values

Specimens	*a* [mm]	N_u^c [kN]	N_u^t [kN]	N_u^c / N_u^t
C5	15	1090.4	1020	1.069
C6	25	1087.9	1100	0.989
C7	40	1455.3	1350	1.078
C8	50	1760.1	1590	1.107

Note: *a = Thickness of the UHPC jackets* N_u^c *= Predicted ultimate load;* N_u^t *= Predicted ultimate load; Ntu = Experimental ultimate load*

load-carrying capacity of RC columns. The tested specimens with connectors achieved substantial strength increases compared with the unstrengthened control column, demonstrating the efficiency of UHPC as a strengthening material.

Acknowledgments

The authors gratefully acknowledge Dr. Tang Shougao, Tongji University, and Professor HouXinlu, Taiyuan University of Technology, for their invaluable support and encouragement. The author also acknowledges the following companies for providing free materials for the experiments: ZHONG CHENG Concrete Inc. and JUCHANG Reinforcement Materials.

REFERENCES

[1] Santos, P., Jùlio, E., Silva, V.: Correlation between concrete to concrete bond strength and the roughness of the substrate surface, Construction and Building Materials, 21 (2007) 8, pp. 1688-1695, https://doi.org/10.1016/j.conbuildmat.2006.05.044

[2] Zanotti, C., Borges, P.H.R., Bhutta, A., et al.: Bond strength between concrete substrate and meta kaolingeo polymer repair mortar: effect of curing regime and PVA fiber reinforcement, Cement & Concrete Composites, 80 (2017), pp. 307-316, https://doi.org/10.1016/j.cemconcomp.2016.12.014

[3] Randl, N.: Design recommendations for interface shear transfer in fib Model Code 2010. Structural Concrete, 14 (2013) 3, pp. 230-241.

[4] OMAR MYM.: Análise Experimental de Pilares de Concreto Armado Reforçados com Concreto Auto-Adensável (CAA). Dissertação (Mestrado), UFG, Goiânia, Goiás, 2006.

[5] Gomes, R.B., Borges, L.L.J., Sahb, K.F.P., Nascimento, P.P.: Reforço de Pilares com Concreto Auto-Adensável e Fibra de Carbono, 49th Congresso Brasileirodo Concreto. Anais. 2007.

[6] Sahb, K.F.P.: Análise Experimental de Pilares de Concreto Armado Submetidos à Flexo-Compressão, Reforçados com Concreto Auto-Adensável e Chumbadores, 224f. Dissertação (Mestrado) UFG, Goiânia, Goiás, 2008.

[7] Nascimento, P.P.: Análise experimental de pilares de concretoarmado submetidos à flexo-compressão, Reforçados com concreto auto- adensável econectores, Dissertacao (Mestrado), UFG, Goiania, Goias, 2009.

[8] Masse, M.B., Bruhwiler, E.: Composite model for predicting the punching resistance of R-UHPFRC-RC composite slabs, Engineering Structure, 117 (2016), pp. 603-616, https://doi.org/10.1016/j.engstruct.2016.03.017

[9] Liu, J., Driver, R.G., Lubell, A.S.: Experimental study on short concrete columns with external steel collars, ACI Structural Journal, 108 (2011) 3, pp. 360-369, https://doi.org/10.14359/51682352

[10] Wu, Y.F., Liu, T., Oehlers, D.J.: Fundamental principles that govern retrofitting of reinforced concrete columns by steel and FRP jacketing, Advances in Structural Engineering, 9 (2006) 4, pp. 507-533, https://doi.org/10.1260/136943306778812769

[11] Minafó, G.: A practical approach for the strength evaluation of RC columns reinforced with RC jackets, Engineering Structure, 85 (2015), pp. 162-169, https://doi.org/10.1016/j.engstruct.2014.12.025.

[12] Alhadid, M.M.A., Youssef, M.A.: Analysis of reinforced concrete beams strengthened using concrete jackets, Engineering Structure, 132 (2017), pp. 172-187, https://doi.org/10.1016/j.engstruct.2016.11.014

[13] FDLarrard, T.S.: Optimization of Ultra-High-Perforance Concrete by the Use of a Packing Model, Cement and Concrete Research, 24 (1994) 6, pp. 997-1009, https://doi.org/10.1016/ 0008-8846(94)90022-1

[14] Shafieifar, M., Farzad, M., Azizinamini, A.: Experimental and Numerical Study on Mechanical Properties of Ultra High Performance Concrete (UHPC), Construction and Building Materials, 156 (2017), pp. 402-411, https://doi.org/10.1016/j.conbuildmat.2017. 08.170.

[15] Wille, K., Naaman, A.E., Parra-Montesinos, G.J.: Ultra-High Performance Concrete with Compressive Strength Exceeding 150MPa (22 ksi): A Simpler Way, ACI Material Journal, 108 (2011) 1, pp. 34-46, https://doi.org/10.1016/j.proeng.2011.11.145

[16] Martinola, G., Meda, A., Plizzari, G.A., Rinaldi, Z.: Strengthening and repair of RC beams with fiber reinforced concrete, Cement and Concrete Composites, 32 (2010) 9, pp. 731-739, https://doi.org/10.1016/j.cemconcomp.2010.07.001

[17] Al-Osta, M.A., Isa, M.N., Baluch, M.H., Rahman, M.K.: Flexural behavior of reinforced concrete beams strengthened with ultra-high performance fiber reinforced concrete, Construction and Building Materials, 134 (2017), pp. 279-296, https://doi.org/10.1016/j.conbuildmat.2016.12.094

[18] Beschi, C., Meda, A., Riva, P.: Column and joint retrofitting with high performance fiber reinforced concrete jacketing, Journal of Earthquake Engineering, 15 (2011) 7, pp. 989-1014, https://doi.org/10.1080/13632469.2011.552167

[19] Meda, A., Mostosi, S., Rinaldi, Z., Riva, P.: Corroded RC columns repair and strengthening with high performance fiber reinforced concrete jacket, Materials and Structures, 49 (2016), pp. 1967-1978, https://doi.org/10.1617/s11527-015-0627-1

[20] Elsayed, M.B., Taye,h B.A., Elmaaty, M.A., Aldahshoory, Y.: Behaviour of RC columns strengthened with Ultra-High Performance Fiber Reinforced concrete (UHPFRC) under eccentric loading, Journal of Building Engineering, 47 (2022), pp. 103857, https://doi.org/10.1016/j.jobe.2021.103857

[21] Paschalis, S.A., Lampropoulos, A.P.: Investigation of key parameters affecting the use of Ultra-High Performance Fiber Reinforced Concrete (UHPFRC) as strengthening material, Structures, 62 (2024), pp. 106257, https://doi.org/10.1016/j.istruc.2024.106257

[22] Aoude, H., Dagenais, F.P., Burrell, R.P., Saatcioglu, M.: Behavior of ultra-high performance fiber reinforced concrete columns under blast loading, International Journal of Impact Engineering, 80 (2015), pp. 185-202, https://doi.org/10.1016/j.ijimpeng.2015.02.006

[23] Dadvar, S.A., Mostofinejad, D., Bahmani, H.: Strengthening of RC columns by ultra-high performance fiber reinforced concrete (UHPFRC) jacketing, Construction and Building Materials, 235 (2020), pp. 117485, https://doi.org/10.1016/j.conbuildmat.2019.117485

[24] Lampropoulos, A., Paschalis, S., Tsioulou, O., Dritsos, S.: Numerical Investigation of Reinforced Concrete (RC) Columns Strengthened with Ultra-High-Performance Fiber-Reinforced Concrete (UHPFRC) Jackets, Materials, 17 (2024) 14, pp. 3380, https://doi.org/10.3390/ma17143380

[25] JGJ/T 101-2015: Specification for Seismic Test of Buildings, China Architecture and Building Press, Beijing, China, 2015.

[26] Vintzeleou, E., Tassios, T.: Mathematical models for dowel action under monotonic and cyclic conditions, Magazine of Concrete Research, 38 (1986) 134, pp. 13-22, https://doi.org/10.1680/MACR.1986.38.134.12

[27] Randl, N., Wicke, M.: Schubübertragung zwischen Alt- und Neubeton. Beton- und Stahlbetonbau, 95 (2000) 8, pp. 461-473.

[28] Randl, N., Münger, F., Wicke, M.: Verstärkung von Brücken tragwerken durch Aufbeton. Bauingenieur, 4 (2005), pp. 207-214.

[29] GB 50010-2010: Code for design of concrete structures, China Architecture and Building Press, Beijing, China, 2010.

[30] Lu, Z.H., Zhao, Y.G., Asce, M.: Empirical stress strain model for unconfined high strength concrete under uniaxial compression, Journal of Materials in Civil Engineering, 2010, pp. 1181-1186, https://doi.org/10.1061/(ASCE)MT.1943-5533.0000095

[31] Hassoun, M.N., Sahebjam, K.: Plastic hinge in two-span reinforced concrete beams containing steel fibers, Canadian Society for Civil Engineering, pp. 119-139, 1985.

[32] Mohammed, A.S., Tamer, M.E., Bothaina, O.: Analysis of RC columns strengthened with ultra-high performance fiber reinforced concrete jackets under eccentric loading, Engineering Structures, 220 (2020), pp. 111016, https://doi.org/10.1016/j.engstruct.2020.111016

[33] Xu, M.X., Liang, X.W., Wang, P., Wang, Z.Y.: Theoretical investigation on normal section flexural capacity of UHPC beams, Engineering Mechanics, 36 (2019) 8, pp. 70-78, https://doi.org/10.6052/j.issn.1000-4750.2018.06.0307

[34] Abrishambaf, A., Pimentel, M., Nunes, S.: Influence of fibre orientation on the tensile behavior of ultra-high performance fibre reinforced cementitious composites, Cement & Concrete Research, 97 (2017): 28-40, https://doi.org/10.1016/j.cemconres.2017.03.007

[35] Mertol, H.C., Rizkalla, S., Zia, P., Mirmiran, A.: Characteristics of compressive stress distribution in high-strength concrete, ACI Structural Journal, 105 (2008) 5, pp. 626-633, https://doi.org/10.14359/19946

[36] Guri, Z., Ristic, J., Ristic, D.: Nonlinear response of RC column models under real earthquakes and axial loads, GRAĐEVINAR, 76 (2024) 10, pp. 919-930, https://doi.org/https://doi.org/10.14256/JCE.3947.2024

[37] Peker, O., Altan, M.F.: Software development for retrofitting columns with FRP composites: A case study, GRAĐEVINAR, 76 (2024) 2, pp. 139-148, https://doi.org/10.14256/JCE.3738.2023

[38] Nechevska-Cvetanovska, G., Roshi, A., Bojadjieva, J., Bojadjiev, J., Trajcevski, Z.: Quasi-static tests on RC building columns strengthened with CFRP, GRAĐEVINAR, 73 (2021) 8, pp. 805-818, https://doi.org/10.14256/JCE. 3087.2020